International Journal of Nanomedicine Dovepress

Open Access Full Text Article ORIGINAL RESEARCH

Direct Labeling of Gold Nanoparticles with Iodine-131 for Tumor Radionuclide Therapy

Meilin Zhu[1], Lingzhou Zhao[2], Xia Lu[2]

[1]School of Basic Medical Sciences, Ningxia Medical University, Yinchuan, Ningxia, 750004, People's Republic of China; [2]Department of Nuclear Medicine, Northern Jiangsu People's Hospital, Clinical Medical College, Yangzhou University, Yangzhou, 225001, People's Republic of China

Correspondence: Xia Lu, Department of Nuclear Medicine, Northern Jiangsu People's Hospital, Clinical Medical College, Yangzhou University, Yangzhou, 225001, People's Republic of China, Tel +86 18051061486, Email lxgf2222@163.com

Purpose: Gold nanoparticles (Au NPs) are widely used as versatile templates to develop multifunctional nanosystems for disease diagnosis and treatment. Iodine can bind to gold via chemisorption, making this a simple method for labeling Au NPs with radioactive iodine. However, the evaluation of tumor radionuclide therapy is insufficient. In this study, we investigated the feasibility of ^{131}I-adsorbed Au NPs as novel nanoprobes for tumor radionuclide therapy.

Materials and Methods: Radiolabeling was performed by mixing Au NPs and ^{131}I, and the radiochemical purity (RCP) and in vitro stability of ^{131}I-adsorbed Au NPs were analyzed under different conditions, including various temperatures, pH values, and ^{131}I concentrations. The tumor accumulation and therapeutic potential of ^{131}I-adsorbed Au NPs were assessed using a subcutaneous tumor model after intratumoral injection.

Results: The data showed that the chemisorption of the Au NPs onto ^{131}I was instant, specific, and quantitative. The ^{131}I-adsorbed Au NPs exhibited high in vitro stability in different media, distinct inhibitory effects on tumor cells in vitro, good retention ability, and therapeutic effects after intratumoral injection into tumor-bearing mice in vivo.

Conclusion: Our work demonstrates that chemisorption of Au NPs and radioiodine has great potential as a strategy for constructing various nanosystems for theranostic applications.

Keywords: gold nanoparticles, iodine-131, chemisorption, radionuclide therapy

Introduction

Radionuclide therapy delivers cytotoxic levels of radiation to specific disease sites and has been widely applied in cancer treatment.[1,2] Unlike conventional radiation therapy, which targets tumors externally, radionuclide therapy uses therapeutic radiopharmaceuticals that specifically bind to tumor tissues at the cellular level, exerting ionizing radiation within tumor cells, causing double-strand DNA damage, and eventually leading to tumor apoptosis.[3,4] Therapeutic radiopharmaceuticals are composed of appropriate radionuclides and tumor target-specific moieties, including antibodies, peptides, and small molecules.[5] Although numerous therapeutic radionuclides have been developed for radionuclide therapy, including but not limited to iodine-125 (^{125}I), iodine-131 (^{131}I), rhenium-188 (^{188}Re), yttrium-90 (^{90}Y), lutetium-177 (^{177}Lu), astatine-211 (^{211}At) and radium-223 (^{223}Ra), ^{131}I is one of the most widely used therapies in clinical application due to its favorable physical properties, safety, and low cost.[6,7]

Advances in cancer nanomedicine have accelerated the use of various nanoparticles (NPs) as versatile carriers for the development of therapeutic radiopharmaceuticals.[8–11] In particular, gold NPs (Au NPs) have emerged as attractive nanoplatforms for tumor radionuclide therapy because of their remarkable physicochemical properties.[12,13] Through facile surface modifications, Au NPs can be synchronously functionalized with targeting ligands and therapeutic radionuclides for superior cancer therapy, which improves tumor uptake and minimizes unnecessary radiation exposure to normal tissues.[14] Meanwhile, the β-particles emitted from radionuclides, such as ^{131}I, can be converted to X-rays via the Bremsstrahlung reaction; these X-rays have a much greater penetration depth than the emitted β-particles, which further strengthen the anti-tumor efficacy.[6,15,16] Therefore, radiolabeled Au NPs possessing synergistic effects in tumor treatment

Received: 30 June 2024
Accepted: 3 November 2024
Published: 13 November 2024

have attracted much interest. To date, we and several other groups have reported different forms of ^{131}I-labeled Au NPs as therapeutic radiopharmaceuticals for tumor therapy via intravenous or intratumoral injection.[17–20] For ^{131}I radiolabeling of Au NPs, certain functional groups are generally essential, such as tyrosine residues, which require appropriate modifications before radiolabeling. Although these modified Au NPs can be effectively labeled with ^{131}I via oxidants with relatively high radiochemical purity (RCP), such as the most commonly used chloramine-T and Iodogen methods, further purification is required.[20–23] Notably, iodine and astatine have strong binding affinities to Au atoms, suggesting that ^{124}I, ^{125}I, ^{131}I and ^{211}At can be easily chemisorbed onto Au NPs.[18,24–30] This chemisorption property may provide a simpler process and higher radiochemical yields for ^{131}I-labeled Au NPs than the radiolabeling method based on redox reactions. Although ^{131}I directly-labeled Au NPs have been successfully used as nanoprobes for tumor-targeted imaging, the studies on the chemisorption and evaluating the feasibility of tumor radionuclide therapy are still insufficient.

Based on the availability and high-affinity interaction between iodine and Au atoms, we conjugated Au NPs with ^{131}I via chemisorption and assessed the feasibility of ^{131}I-chemisorbed Au NPs for tumor treatment. The radiolabeling and RCP analysis of ^{131}I-adsorbed Au NPs were carefully performed at different temperatures, pH values, and ^{131}I concentrations. The in vitro stability of ^{131}I-adsorbed Au NPs was analyzed in different media. The tumor accumulation and therapeutic potential of ^{131}I-adsorbed Au NPs were assessed using a subcutaneous tumor model after intratumoral injection.

Materials and Methods

Materials

PEI-Au NPs, Glu-Au NPs, PEG-Au NPs, BSA-Au NPs, Au NPs (5 nm), Au NPs (20 nm) and Au NPs (100 nm) were purchased from Xi'an ruixi Biological Technology Co., Ltd (Xi'an, China). Na^{131}I solution was supplied by Shanghai GMS Pharmaceutical Co., Ltd (Shanghai, China). Dulbecco's Modified Eagle's Medium (DMEM), FBS, penicillin, streptomycin, chloramine T and Cell Counting Kit-8 (CCK-8) were provided from Shanghai Dobio Biotech CO., Ltd (Shanghai, China). C6 cells (a rat glioma cell line) were provided from Institute of Biochemistry and Cell Biology (the Chinese Academy of Sciences, Shanghai, China). Female BALB/c nude mice (4–6 weeks old, 18–20 g) were purchased from Shanghai Slac Laboratory Animal Center (Shanghai, China).

Preparation of ^{131}I-Absorbed Au NPs

Typical radiolabeling was performed by simply mixing Au NPs (200 μL, 1 mg/mL) with Na^{131}I (100 μL, 10 mCi/mL) at 37 °C for 30 min. A series of radiolabeling experiments using PEI-Au NPs and Au NPs (5 nm) were further carried out at different conditions, including various temperatures (4–100 °C), pH values (1–13), and ^{131}I concentrations (1–10^4 μCi/mL). The RCPs of the ^{131}I-absorbed Au NPs were assessed via instant thin-layer chromatography (ITLC) according to the protocols reported in our previous work.[17] Furthermore, to evaluate the specificity of chemisorption, ^{131}I radiolabeling was performed in the presence of excess cold iodide, KI, or NaCl, and the ^{131}I-absorbed Au NPs were incubated with these chemical reagents for 5 min at room temperature. Moreover, considering the influence of the oxidation state of ^{131}I on chemisorption, an excess oxidant (chloramine-T, 5 mg/mL) was added to the Na^{131}I solution before and after mixing with the PEI-Au NPs and Au NPs (5 nm). RCPs were assessed using the ITLC method described above.

In vitro Stability Study

The stability of ^{131}I-absorbed Au NPs (5 nm) and ^{131}I-absorbed PEI-Au NPs in vitro was studied by measuring the RCPs via ITLC under different conditions. Specifically, their RCPs in PBS solution (pH = 7.4) were analyzed at room temperature for 28 d, and a similar procedure was applied in 50% FBS at 37 °C for 7 d. To assess the influence of acidity, alkalinity, and oxidants on the stability of ^{131}I-absorbed Au NPs, the RCPs were tested at various pH values (1–13) and in the presence of chloramine-T (5 mg/mL) at room temperature for 7 d.

Cells and Animal Models

C6 cells were regularly cultured in Dulbecco's Modified Eagle Medium supplemented with 10% FBS, penicillin (100 U/mL), and streptomycin (100 U/mL) in a humidified incubator with 5% CO_2 at 37 °C. A subcutaneous tumor model was established by subcutaneously injecting 1×10^6 C6 cells into the right flank of each mouse. The mice were regularly raised for 2–3 weeks in specific pathogen-free environment, and when tumor volumes reached 0.5−1.0 cm^3, these tumor-bearing mice were used for in vivo experiments. All animal studies and experimental procedures were approved by the Laboratory Animal Ethics Committee of Yangzhou University (No.202404019), and conducted in accordance with the ethical standards of the National Health and Medical Research Council (China).

Cytotoxicity Assay

A CCK-8 assay was used to analyze the cytotoxicity of Au NPs (5 nm) and PEI-Au NPs before and after ^{131}I labeling in C6 cells. Briefly, C6 cells were seeded into 96-well plates (1×10^4 cells/well) and incubated overnight. These cells were then treated with Au NPs at different concentrations (0, 6.25, 12.5, 25, 50, and 100 μg/mL). After incubation for 48 h, the cell viability of each group was measured using the CCK-8 assay according to standard procedures. Similarly, the cytotoxicity of ^{131}I-absorbed Au NPs in C6 cells were evaluated at different radioactive concentrations (0, 10, 50, 100, 500, and 1000 μCi/mL, respectively). After incubation for 48 h, the viability of the C6 cells was determined using the CCK-8 assay.

In vivo SPECT Imaging

To assess the retention ability of the ^{131}I-absorbed Au NPs in tumors, the mice were intravenously and intratumorally injected with a PBS solution of ^{131}I-absorbed Au NPs (5 nm) and ^{131}I@PEI-Au NPs (^{131}I = 30 mCi/mL, 30 μL); mice injected with Na^{131}I at the same dose were set as a control for comparison. These tumor-bearing mice were imaged at 1 min and 0.5, 3, 6, 12, and 24 h post-injection using an Infinia GE SPECT imaging system containing a SPECT scanner, high-energy general-purpose collimators, and Xeleris 2.0 Work Station.

In vivo Antitumor Efficacy

To evaluate the in vivo anti-tumor efficacy of ^{131}I-absorbed Au NPs, the tumor-bearing mice were randomly divided into six groups (six mice per group) and intratumorally injected with 30 μL of ^{131}I@Au NPs (5 nm), ^{131}I@PEI-Au NPs, Na ^{131}I, PEI-Au NPs, Au NPs (5 nm), or saline at a ^{131}I concentration of 30 mCi/mL or an Au concentration of 1 mg/mL. Before the animal experiments, the tumor-bearing mice were fed water containing KI (1%) for 3 d to block the thyroid uptake of ^{131}I. The body weight of each mouse was recorded, and the tumor volumes were calculated every 3 d according to the following formula: (tumor length× (tumor width)^2)/2. To assess the antitumor efficacy and potential toxicity of ^{131}I-absorbed Au NPs, one mouse from each group was euthanized using an overdose of anesthetics after 15 d of treatment to obtain the major organs (heart, liver, spleen, lung, and kidneys) and subcutaneously implanted tumors for H&E staining. To further evaluate the degree of apoptosis in treated tumor-bearing mice, tumor tissues were stained using a TUNEL assay.

Biochemistry Analysis

Ten healthy ICR mice were randomly divided into two groups (n = 5) and intravenously injected with ^{131}I@PEI-Au NPs (^{131}I = 4.5 mCi/mL, 200 μL) and PEI-Au NPs ([Au] = 1 mg/mL, 200 μL), respectively. Another 5 healthy ICR mice injected with 200 μL saline were used as control. The blood samples were collected at 14 days post-injection. The biochemistry parameters including alkaline phosphatase (ALP), alanine aminotransferase (ALT), aspartate aminotransferase (AST), blood uric acid (BUA) and blood urea nitrogen (BUN) were analyzed.

Statistical Analysis

The data in this study were presented as the mean ± standard deviation and analyzed via one-way analysis of variance. The final data were marked with (*) for $P < 0.05$, (**) for $P < 0.01$, and (***) for $P < 0.001$. Statistical significance was set at $P < 0.05$.

Results and Discussion

Instantaneous Chemisorption of Au NPs to ^{131}I

Au NPs have demonstrated their versatility as platforms for cancer theranostic applications owing to their good biocompatibility, simple synthesis, and controllable modifications.[31,32] With the development of nanomedicine, various radionuclides have been used to construct multifunctional Au NPs, such as ^{64}Cu, ^{68}Ga, and ^{99m}Tc, as well as radionuclides of iodine, including ^{124}I, ^{125}I, and ^{131}I.[33–38] In most cases, appropriate bifunctional chelators, such as DOTA, NOTA, or HYNIC, must be modified on the surface of Au NPs before radiolabeling. Similarly, certain functional groups are necessary for direct radioiodine labeling via redox chemistry, such as tyrosine. Based on this strategy, various ^{131}I-labeled multifunctional Au NPs have been successfully established for targeted tumor imaging and radionuclide therapy in numerous studies.[6,19–22] Notably, potent Au-I bonds can be formed through chemisorption because of the high affinity and strong binding of iodine to the surface of Au NPs.[24,39] This simple chemistry enables the straightforward and efficient radiolabeling of ^{131}I on Au NPs without oxidants or functional groups.

In this study, the chemisorption of ^{131}I was investigated using several types of Au NPs, including colloidal Au NPs with different diameters (5, 20, and 100 nm) and Au NPs (5 nm) modified with polyethyleneimine (PEI-Au NPs), glucose (Glu-Au NPs), polyethylene glycol (PEG-Au NPs), and bovine serum albumin (BSA-Au NPs). In a routine radiolabeling experiment, 100 μL of Na^{131}I solution (10 mCi/mL) was mixed with 200 μL of phosphate-buffered saline (PBS) solution (0.1 M, pH 7.4) containing these Au NPs (1 mg/mL) at 37 °C for 30 min, which was a typical reaction condition used in our previous study.[16] Unexpectedly, the RCPs were nearly 100% (n = 3) under these conditions (Figure 1A). Moreover, the same results were achieved at room temperature within 2 min, suggesting a higher radiolabeling efficiency than that of conventional methods. Notably, the effective ^{131}I radiolabeling of PEI-, glucose-, PEG-, and BSA-coated Au NPs implied that these modifications on Au NPs had little effect on ^{131}I adsorption. Additionally, after testing various reaction times of 0.5, 1, 5, and 15 min, we found that ^{131}I radiolabeling was rapidly completed with 100% RCPs after simply mixing for 0.5 min (Figure 1B). This observation indicates that the chemisorption of ^{131}I to the Au NPs occurred instantaneously.

Specific Chemisorption of Au NPs to ^{131}I

Chloramine-T has been widely used as an oxidizing agent for radioiodine radiolabeling because of its high efficiency, good repeatability, and low cost. It hydrolyzes the hypochlorous acid in water and oxidizes iodine ions to iodine molecules (I_2). To evaluate the chemisorption specificity, ^{131}I ions were first oxidized using chloramine-T. When Au NPs were added to a mixture of Na^{131}I and chloramine-T, few ^{131}I-absorbed Au NPs were found, indicating that Au NPs could specifically chemisorb ^{131}I ions rather than ^{131}I molecules (Figure 1C). Conversely, when chloramine-T was added to the prepared ^{131}I-absorbed Au NPs, no obvious changes were observed in the RCPs, suggesting that the ^{131}I chemisorbed onto the Au NPs could not be further oxidized by chloramine-T (Figure 1C). This situation should be considered in the process of radiolabeling when using the chloramine-T method because distinguishing whether the connection between Au NPs and ^{131}I is chemisorption or covalent bonding is difficult.

To further confirm that the binding to Au NPs was due to the chemisorption of iodine and not ionic binding, several chemicals, including I_2, KI, and NaCl, were used to inhibit ^{131}I radiolabeling. The data showed that Au NPs absorbed more than 99% ^{131}I ions in the presence of NaCl but less than 1% in the presence of I_2 or KI (Figure 1D). These chemicals were also used to desorb ^{131}I-absorbed Au NPs after incubation for 5 min at room temperature. As expected, I_2 and KI had strong desorptive capacities and nearly total desorption of ^{131}I was observed, whereas NaCl had no effect (Figure 1E). Moreover, no chemisorption was observed between the Au NPs and ^{68}Ga,[18] F, or ^{99m}Tc ions, further supporting the selective capture of radioiodine (Figure 1F).

Factors Influencing Chemisorption

Before radioiodine radiolabeling, several factors must be considered, such as the source of radioiodine, structural characteristics of the radiolabeling precursor, pH, temperature, and volume. Generally, a fresh radioiodine source with a high radioactivity concentration (> 50 mCi/mL) is preferred. In this study, the concentration of the Na^{131}I solution used

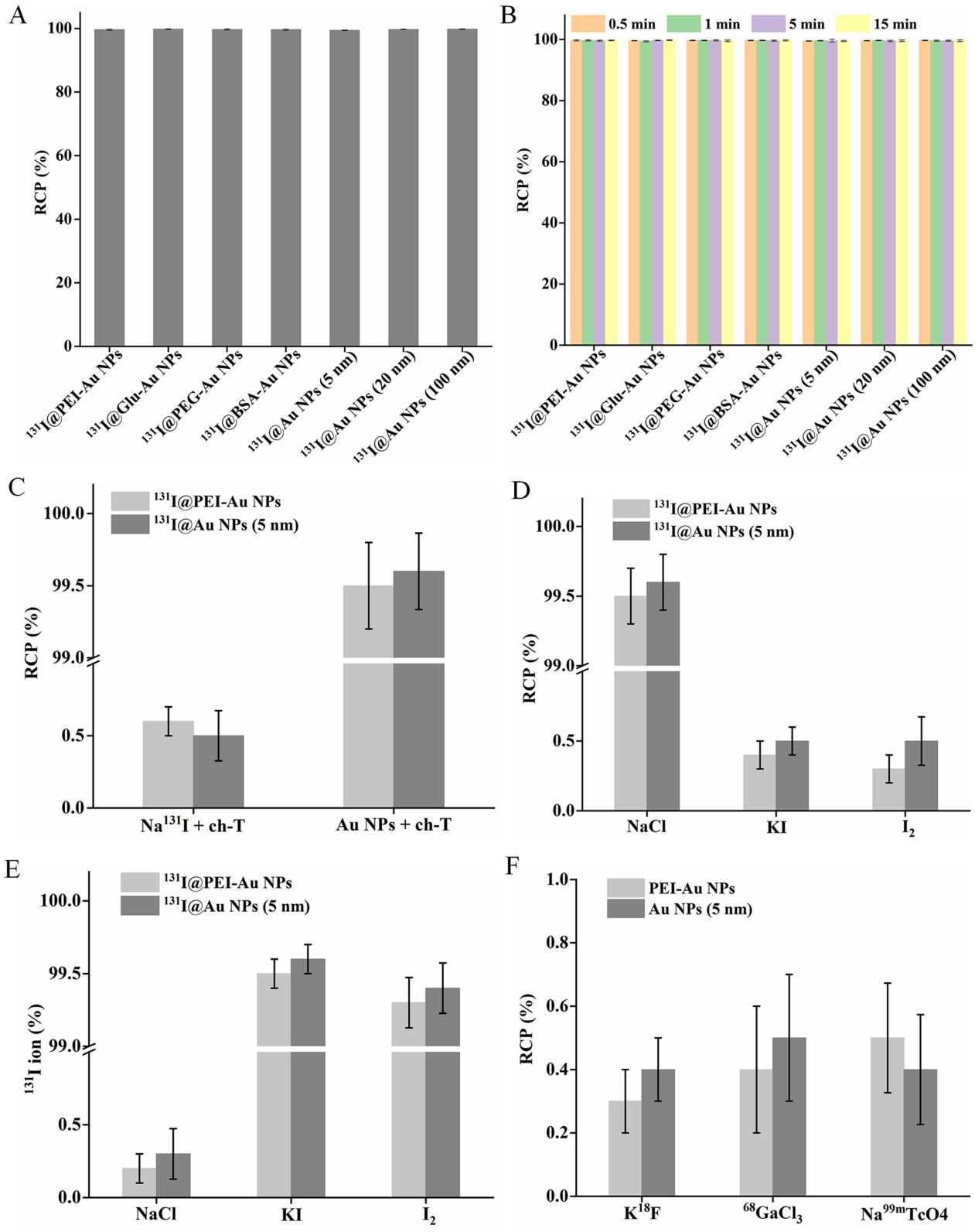

Figure 1 Instantaneous and specific chemisorption of Au NPs to ^{131}I. (**A**) The RCP of these ^{131}I@PEI-Au NPs, ^{131}I@Glu-Au NPs, ^{131}I@PEG-Au NPs, and ^{131}I@BSA-Au NPs, as well as ^{31}I@Au NPs with diameters of 5, 20, and 100 nm at 37 °C for 30 min. (**B**) The RCPs of these ^{131}I@Au NPs at room temperature for 0.5, 1, 5, and 15 min. (**C**) The RCPs of ^{131}I@PEI-Au NPs and ^{131}I@Au NPs (5 nm) after mixing with Na^{131}I and chloramine-T. (**D**) The RCPs of ^{131}I@PEI-Au NPs and ^{131}I@Au NPs (5 nm) in the presence of chloramine-T, NaCl, KI, and I_2. (**E**) Desorption of ^{131}I from Au NPs by NaCl, KI, and I_2 solutions. (**F**) Chemisorption between Au NPs and ^{68}Ga, ^{18}F, and ^{99m}Tc ions.

for radiolabeling was more than 100 mCi/mL, which is conducive for the utilization of radioiodine. To investigate the influence of nanoparticle size on ^{131}I radiolabeling, colloidal Au NPs with diameters of 20 and 100 nm were used as controls. As expected, the 5-nm Au NPs showed the highest RCPs, and the 20-nm Au NPs had higher RCPs than that of the 100-nm Au NPs at an Au concentration of 40 μg/mL (Figure 2A). This observation can be explained by the larger specific surface area of the 5-nm Au NPs, indicating a better chemisorption capacity of Au NPs with sizes smaller than ^{131}I. This finding was consistent with the significantly higher RCPs of the PEI-Au NPs than those of the 20- and 100-nm Au NPs under the same conditions, because the mean diameter of the PEI-Au NPs was approximately 5 nm.[17]

To evaluate the adsorption properties of Au NPs for ^{131}I at different reaction conditions, a series of ^{131}I radiolabeling experiments of Au NPs (5 nm) and PEI-Au NPs were carried out at the different pH values (pH = 1–13), temperatures (4, 25, 70 and 100 °C), and ^{131}I concentrations (1–10^4 μCi/mL). The data showed that free ^{131}I ions could only be detected at 100 °C (with relatively high RCPs of more than 95%), and the RCPs were able to reach 100% as the temperature of the reaction mixture decreased to 70 °C, indicating the powerful absorbability of Au NPs to ^{131}I (Figure 2B). Moreover, the adsorption capacities of the Au NPs to ^{131}I were excellent under various pH conditions (pH = 1–13) at room temperature. These results showed that all the RCPs were greater than 99%, suggesting that the chemisorption of ^{131}I to Au NPs could be efficiently implemented over a wide pH range (Figure 2C). Likewise, the high RCPs were also observed at different

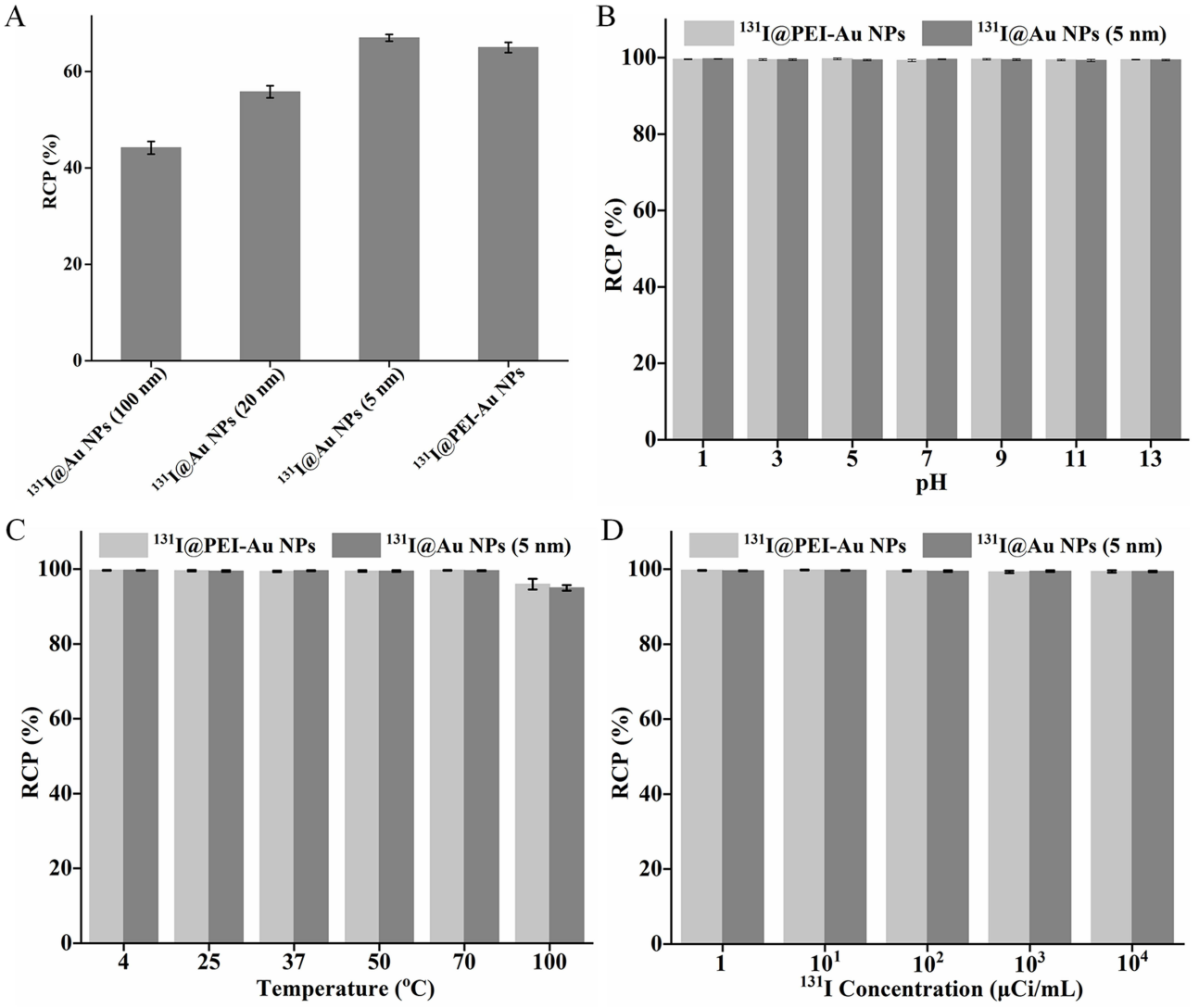

Figure 2 Factors influencing chemisorption of Au NPs to ^{131}I. (**A**) The RCPs of ^{131}I@PEI-Au NPs and ^{131}I@Au NPs with diameters of 5, 20, and 100 nm at an Au concentration of 40 μg/mL. The RCPs of ^{131}I@PEI-Au NPs and ^{131}I@Au NPs (5 nm) at the different (**B**) pH values, (**C**) temperatures, and (**D**) ^{131}I concentrations.

Table 1 Comparison Between the Routine Radiolabeling Methods and Chemisorption

	Chloramine T Method	IOGOGEN Method	Chemisorption
Oxidizing agent	Chloramine T	IOGOGEN	None
Chemical bond	C-I	C-I	Au-I
Temperature	≤ 37 °C	≤ 37 °C	≤ 100 °C
pH	7–8	6–9	1–13
Time	Tens of seconds to minutes	Several minutes	Almost instantaneous
Volume	≤ 1 mL	≤ 1 mL	Up to 300 mL
Termination reaction	$Na_2S_2O_5$	None	None
Purification	Necessary	Necessary	None

^{131}I concentrations (1–10^4 μCi/mL, Figure 2D). In general, ^{131}I concentration and reaction volume are important factors in oxidant-based ^{131}I radiolabeling strategies; low concentrations or large volumes are not recommended because of low ^{131}I utilization efficiency and specific radioactivity. In our previous study, the ^{131}I concentrations were above 1×10^4 μCi/mL and the total reaction volumes were less than 1 mL, resulting in relatively high RCPs of 60% to 80%.[17] In this study, after mixing 10 μL of Na^{131}I solution and 20 μL of Au NP (5 nm) or PEI-Au NP solution, the ^{131}I concentration was 1×10^4 μCi/mL with RCPs of up to 100%. Notably, even when the ^{131}I concentration was diluted 10,000-fold 1 μCi/mL with a total volume of 300 mL, namely, the RCPs remained stable, suggesting that Au NPs could efficiently chemisorb ^{131}I ions at very low concentrations and that high ^{131}I utilization was maintained regardless of the reaction volume. A comparison between the chemisorption in this study and the routine radiolabeling methods is provided in Table 1.

Correlation Between RCP and Au NP Concentration

To further assess the correlation between RCP and Au NPs concentration, 100 μL of Na^{131}I solution (1 mCi) was individually mixed with 100 μL of Au NPs (5 nm) and PEI-Au NPs at different Au concentrations (0.5–80 μg/mL). After incubation for 1 min at room temperature, the RCPs were immediately evaluated and showed good correlation with Au concentrations in the range of 0.5–60 μg/mL ($r^2 = 0.998$, $P < 0.001$, Figure 3). Notably, the RCPs of ^{131}I@Au NPs (5 nm) and ^{131}I@PEI-Au NPs at 60 μg/mL were 96.2 ± 1.2% and 97.1 ± 0.6% (n = 3), respectively, which could be further raised to 99.9% at 80 μg/mL. This observation suggests that the absorption between ^{131}I and Au NPs might reach equilibrium and that excess Au NPs could further chemisorb free ^{131}I to prompt complete radiolabeling.

In vitro Stability and Cytotoxicity Assays

The Au NPs were absorbed with ^{131}I simply by mixing for 1 min, and high RCPs were acquired. To evaluate whether ^{131}I could be separated from the Au NPs, the long-term radiostability of ^{131}I-absorbed Au NPs was tested under different conditions. The formed ^{131}I-absorbed Au NPs in PBS solution at room temperature showed negligible changes in their RCPs during the study period of 28 d (Figure 4A) and retained RCPs of 99% after exposure to 50% fetal bovine serum (FBS) at 37 °C for 1 week (Figure 4B), indicating excellent stability in vitro. Moreover, no significant change in the RCPs was found in the formed ^{131}I-absorbed Au NPs under various pH values (Figure 4C) or in excess chloramine-T (Figure 4D) at room temperature for 7 d, revealing favorable stability under acidic, alkaline, and oxidant conditions.

The potential cytotoxicity of the Au NPs (5 nm) and PEI-Au NPs before and after ^{131}I radiolabeling was assessed using a Cell Counting Kit-8 (CCK-8) assay. The viability of C6 cells treated with Au NPs (5 nm) and PEI-Au NPs remained high (>90%) at Au concentration range of 0–100 ug/mL, similar to that observed in the PBS control group (Figure 4E). These results indicate that the Au NPs (5 nm) and PEI-Au NPs prior to ^{131}I labeling were not cytotoxic to C6 cells in the given concentration range. In contrast, the viability of C6 cells gradually decreased with increased radioactivity concentration (Figure 4F), and both ^{131}I@Au NPs (5 nm) and ^{131}I@PEI-Au NPs exerted distinct inhibitory

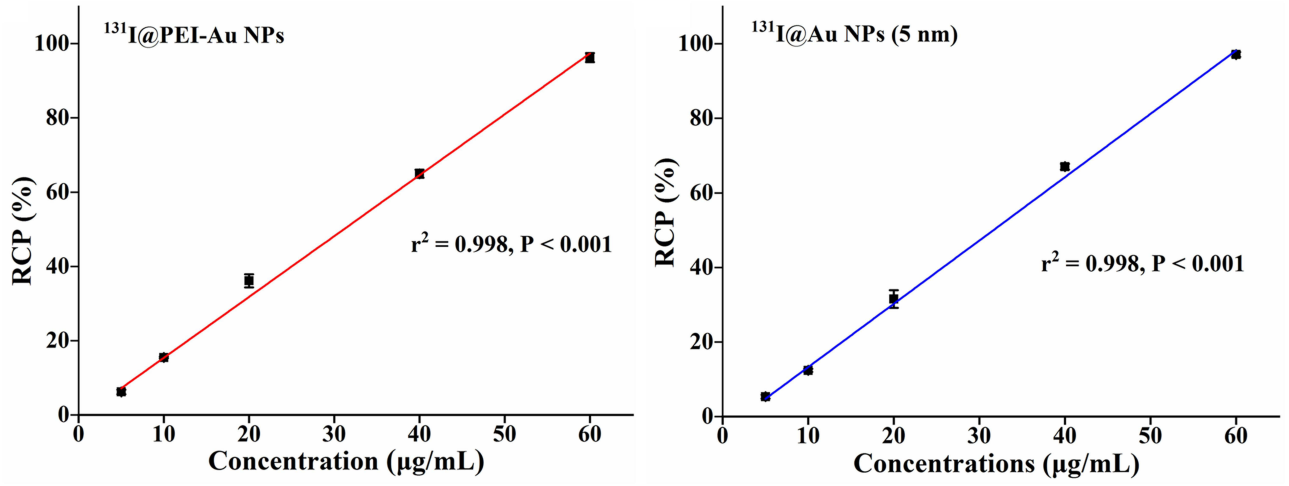

Figure 3 Relationship between the RCPs of PEI-Au NPs and Au NPs (5 nm) at Au concentrations of 0.5–60 μg/mL.

effects compared with that of Na ^{131}I at the radioactivity concentrations of 500 and 1000 μCi/mL, suggesting that ^{131}I-absorbed Au NPs might be internalized into C6 cells through an endocytosis process and exert strong cytotoxicity.

Intratumoral Retention of ^{131}I-Absorbed Au NPs

Single-photon emission computed tomography (SPECT) imaging has great advantages with respect to sensitivity and quantitation, as it can not only directly show the biodistribution of ^{131}I-labeled Au NPs but also estimate the radioactivity in tumor sites or specific organs. To evaluate the intratumoral retention ability, tumor-bearing mice were intratumorally injected with ^{131}I@PEI-Au NPs; Na^{131}I was used as a control. As shown in Figure 5A, during the study period, the ^{131}I@PEI-Au NPs mainly accumulated at the injection sites with low uptake in the liver and kidneys and increased radioactivity in the thyroid, indicating instability in vivo. Despite the insignificant difference in tumor SPECT signal intensities between the ^{131}I@PEI-Au NP and Na^{131}I groups at 1 min post-injection owing to the fast clearance of Na^{131}I from tumors, high radioactivity accumulated over time in the thyroid, kidneys, and bladder, and only the thyroid could be clearly visualized at 24 h post-injection (Figure 5B). These data suggest that ^{131}I@PEI-Au NPs are restricted to tumor tissues with slow metabolism. The tumor accumulation and retention of ^{131}I@PEI-Au NPs were further confirmed by the quantitative analysis of radioactivity in the tumors and thyroid. The relative radioactivity of the tumors at different time points is shown in Figure 5C. At 1 min post-injection, the radioactivity of Na^{131}I in tumors was close to 100%, while the radioactivity was reduced to 25.49 ± 2.38% and 5.99 ± 0.56% at 0.5 and 3 h post-injection, respectively. Less than 2% Na^{131}I could be found in the tumor at 24 h post-injection. Conversely, ^{131}I@PEI-Au NPs displayed good radioactivity retention in the tumor. Although the intratumoral radioactivity of ^{131}I@PEI-Au NPs weakened over time, probably due to their instability in vivo, the remaining proportion of ^{131}I@PEI-Au NPs was larger than that of Na^{131}I at 1 min post-injection, and approximately 20% ^{131}I@PEI-Au NPs remained in the tumor at 24 h post-injection. These data suggest that the radiation-deposition function of the Au NPs was able to withhold ^{131}I with long tumor retention, which could be beneficial for inner tumor irradiation. To further evaluate the intratumoral retention ability of ^{131}I@PEI-Au NPs, thyroid-to-tumor (Th/Tu) SPECT signal ratios at different time points were analyzed (Figure 5D). In contrast to the stable Th/Tu ratios in the ^{131}I@PEI-Au NPs group, those in the Na^{131}I group increased continuously over time and were higher at each time point. At 24 h post-injection, the Th/Tu ratio in the Na^{131}I group was up to 22.31 ± 2.31, which was much higher than the corresponding 0.83 ± 0.26 of ^{131}I@PEI-Au NPs at the same time point, supporting the good intratumoral retention of ^{131}I@PEI-Au NPs. Notably, the tumor retention of ^{131}I-absorbed Au NPs might be further enhanced by optimizing sizes and shapes or modifying various tumor-targeting ligands, which have been proved as effective strategies.[40–42]

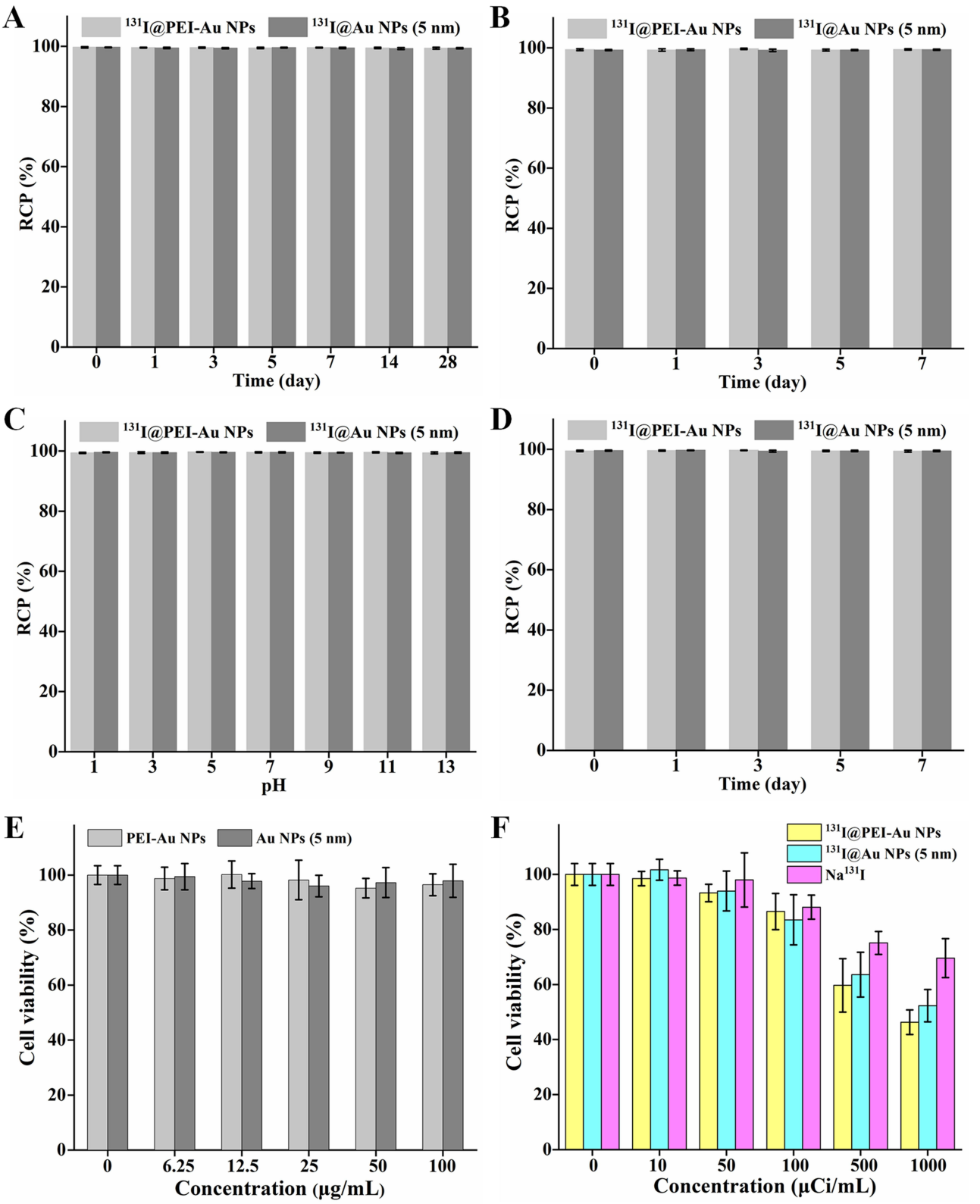

Figure 4 In vitro stability and cytotoxicity of ^{131}I-absorbed Au NPs. The RCP of ^{131}I@PEI-Au NPs and ^{131}I@Au NPs (5 nm) (**A**) in phosphate-buffered saline at room temperature for 28 d, (**B**) in 50% fetal bovine serum at 37 °C, and (**C**) under various pH values or (**D**) in excess chloramine-T at room temperature for 7 d. (**E**) CCK-8 assay of C6 cells treated with PEI-Au NPs or Au NPs (5 nm) at different Au concentrations (0–100 μg/mL) for 48 h. (**F**) CCK-8 assay of C6 cells treated with ^{131}I@PEI-Au NPs, ^{131}I@Au NPs (5 nm), or Na^{131}I at different ^{131}I radioactive doses (0–1000 μCi/mL) for 48 h.

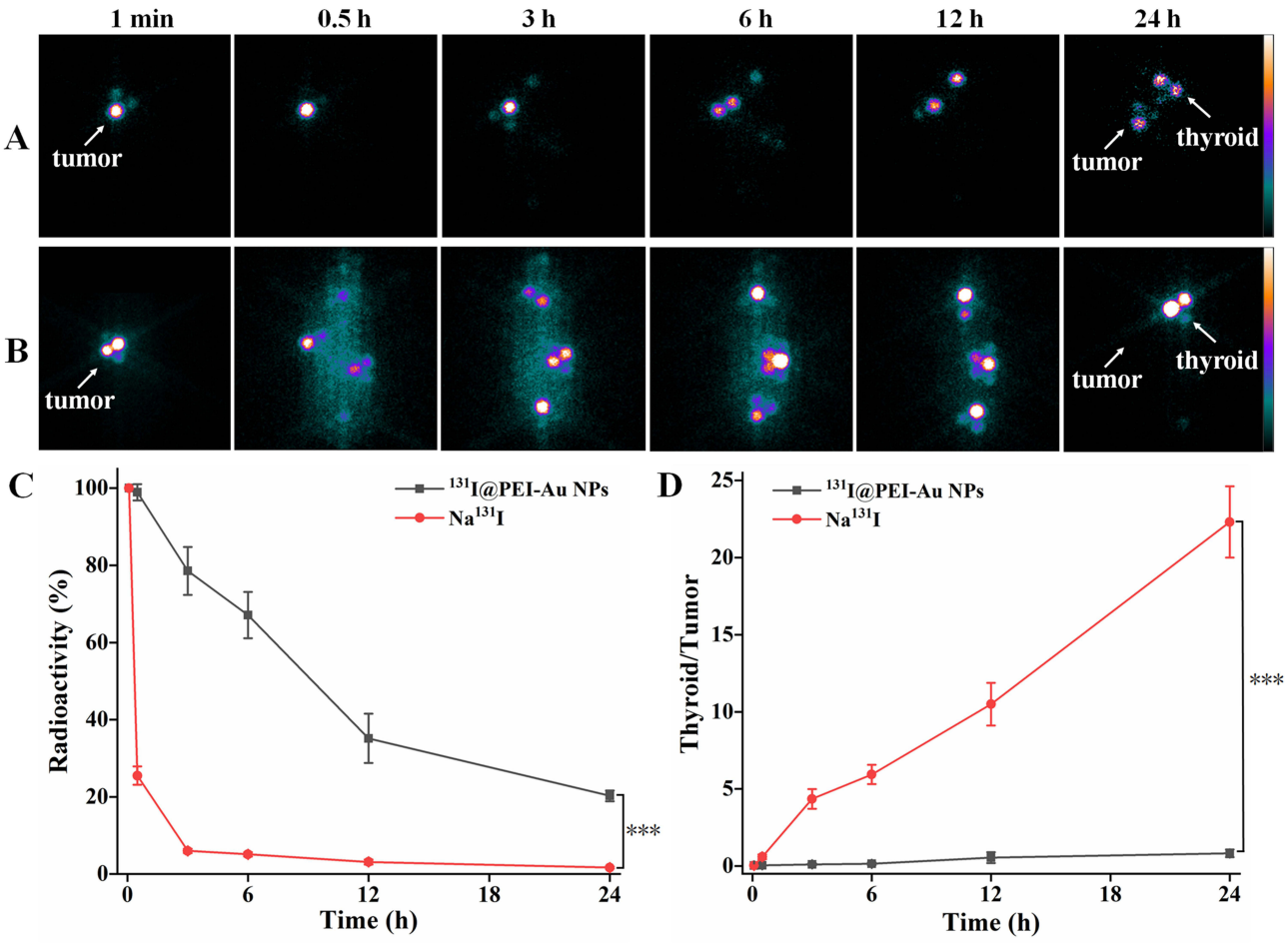

Figure 5 Tumor retention of ^{131}I-absorbed Au NPs after intratumor injection. SPECT images of C6 tumor-bearing nude mice after intratumoral injection of (**A**) ^{131}I@PEI-Au NPs and (**B**) Na^{131}I. (**C**) The relative radioactivity of these nanoparticles in tumors and (**D**) thyroid-to-tumor ratios at different time points. *** $P < 0.001$.

The behavior of ^{131}I@PEI-Au NPs in vivo after intravenous injection was also studied. As expected, neither ^{131}I@PEI-Au NPs nor Na^{131}I showed any apparent tumor uptake during the study period (Figure S1). ^{131}I@PEI-Au NPs mainly accumulated in the liver and spleen, and a small amount of radioactivity was detected in the thyroid, which was related to the in vivo instability and lack of targeting ability of ^{131}I@PEI-Au NPs (Figure S1A). In contrast, most of the Na^{131}I was found in the kidneys and thyroid. The gradually enhanced radioactive signal in the bladder indicated that Na^{131}I was excreted through the urinary system, and only the thyroid gland was visible 12 h post-injection (Figure S1B). In addition, Au NPs can be endowed with imaging and radiotherapy functions by directly incorporating ^{198}Au or ^{199}Au isotopes into the crystal lattices of Au NPs.[40–46] Compared to ^{131}I-absorbed Au NPs, these ^{198}Au- or ^{199}Au-radiolabeled NPs not only showed excellent in vitro stability but also were high stable in vivo (Table 2). Meanwhile, more studies need to be focused on further improving the targeting specificity and biodistribution of these Au NPs for higher tumor uptake and less accumulation in liver and spleen.

Table 2 The Stabilities of Radiolabeled Au NPs in vitro and in vivo

Radionuclide	In vitro	In vivo	Reference
^{198}Au or ^{199}Au	High	High	40–46
^{125}I or ^{131}I	High	Moderate	17–22,24–27

Radionuclide Therapy

Radionuclide therapy has been identified as an effective way for tumor treatment, and currently, ^{131}I is one of the most widely used therapeutic radionuclides in clinical practice.[13] Au NPs have shown great potential in the search for novel ^{131}I-labeled radiopharmaceuticals for cancer therapy. In our previous studies, because of the high density of amines and good water solubility of PEI, we used this versatile macromolecule to manufacture PEI-entrapped Au NPs for tumor radionuclide therapy.[17,22] The manufactured PEI-Au NPs were easily functionalized with targeting molecules and labeled with ^{131}I via the chloramine-T method after modifying the tyrosine residues on their surfaces. In this study, unlike traditional radiolabeling strategies, ^{131}I was chemisorbed onto the surface of PEI-Au NPs with a very high RCP and stability in vitro. However, considering the low tumor uptake and in vivo instability of ^{131}I@PEI-Au NPs after intravenous injection, their potential for tumor therapy was assessed using a single intratumoral injection. After treatment for 15 d, both ^{131}I@PEI-Au NPs and ^{131}I@Au NPs (5 nm) exhibited obvious tumor inhibition efficiency (Figure 6A), whereas mice treated with PEI-Au NPs, Au NPs (5 nm), and Na^{131}I showed exponential tumor growth rates that were similar to those seen with saline treatment with no therapeutic effect. The growth-inhibitory effect followed the order of ^{131}I@PEI-Au NPs (5.04 ± 2.12 times) ≈ ^{131}I@Au NPs (5 nm, 5.93 ± 1.98 times) > PEI-Au NPs (12.88 ± 1.15 times) ≈ Au NPs (5 nm, 13.11 ± 1.11 s times) ≈ Na^{131}I (12.36 ± 2.44 times) ≈ saline (12.33 ± 2.46 times). This finding suggests that tumor radiotherapeutic efficacy is only related to the presence of ^{131}I. Additionally, the antitumor efficacy of ^{131}I-absorbed Au NPs was further demonstrated by the survival rates of mice. As shown in Figure 6B, a longer survival time was observed in mice treated with ^{131}I-absorbed Au NPs than in mice in the other groups. After treatment, 20% of the tumor-bearing mice treated with ^{131}I@PEI-Au NPs and ^{131}I@Au NPs (5 nm) survived for 31 and 30 d, respectively, whereas those treated with Na^{131}I survived for 19 d. Additionally, 100% of the mice treated with saline were dead at 16 d, and no significant differences were observed among the PEI-Au NPs, Au NPs (5 nm), Na^{131}I, and saline treatments in terms of survival rates. In conclusion, the survival time of tumor-bearing mice was effectively extended using ^{131}I-absorbed Au NPs, which can be attributed to ^{131}I retention in tumors. Additionally, the body weights of the mice

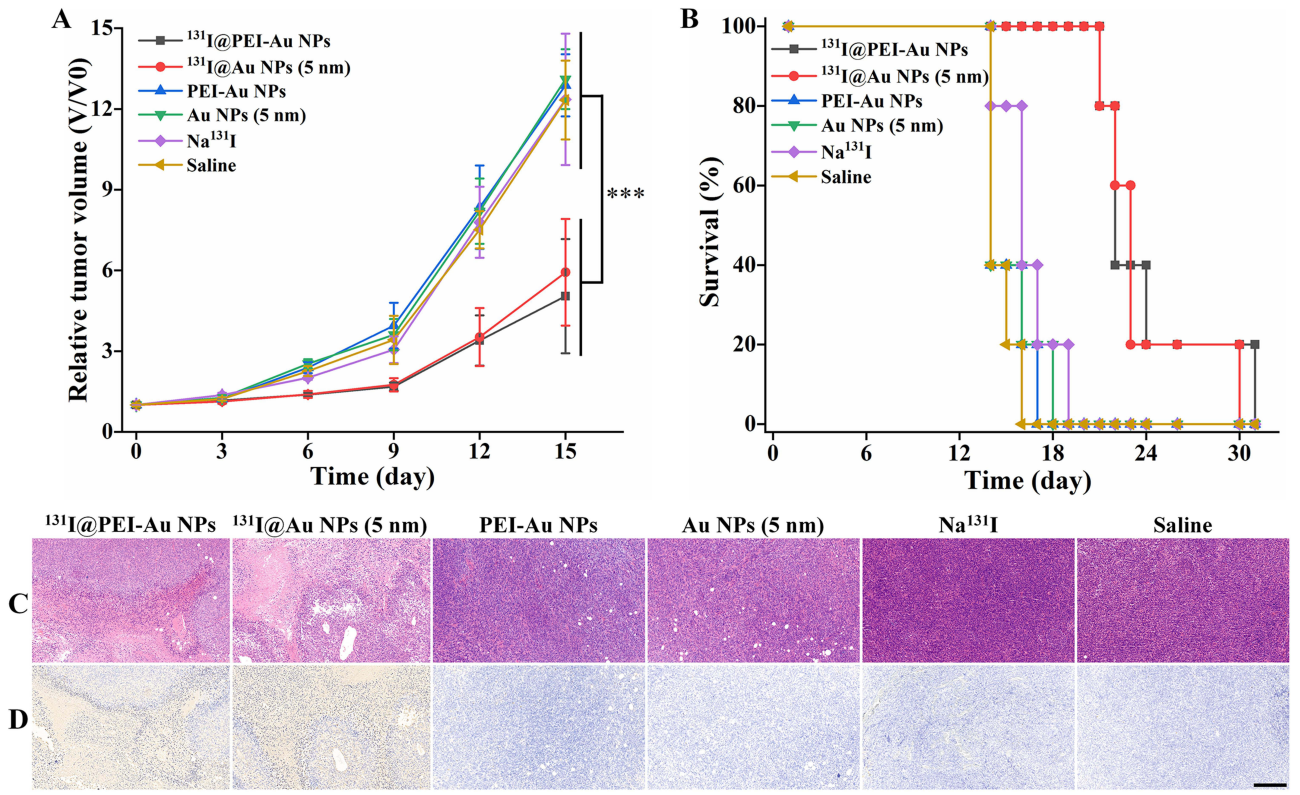

Figure 6 Radionuclide therapy of ^{131}I-absorbed Au NPs. (**A**) Relative tumor volume, (**B**) survival rate, (**C**) Hematoxylin and eosin staining, and (**D**) terminal deoxynucleotidyl transferase dUTP nick end labeling assay of C6 xenografts after different treatments. The scale bar represents 200 μm for all panels. *** P < 0.001.

treated with ^{131}I@PEI-Au NPs, ^{131}I@Au NPs (5 nm), PEI-Au NPs, Au NPs (5 nm), Na^{131}I, or saline showed no significant change (Figure S2), indicating acceptable biocompatibility of the generated ^{131}I-absorbed Au NPs in vivo.

To further evaluate the radiotherapeutic effects and safety of ^{131}I-absorbed Au NPs in vivo, hematoxylin and eosin (H&E) and terminal deoxynucleotidyl transferase dUTP nick end labeling (TUNEL) staining were performed. As shown by H&E staining (Figure 6C), necrotic areas were found only in tumors treated with ^{131}I-labeled materials, while tumors treated with ^{131}I@PEI-Au NPs displayed necrotic areas similar to those treated with ^{131}I@Au NPs (5 nm). The same results were observed using TUNEL staining. Positive staining of apoptotic cells was only found in the tumors treated with ^{131}I@Au NPs (5 nm) and ^{131}I@PEI-Au NPs (Figure 6D). Taken together, the H&E and TUNEL staining data demonstrated that ^{131}I-absorbed Au NPs are a promising nanoplatform for inhibiting tumors by promoting the apoptosis and necrosis of tumor cells. Additionally, the systemic toxicity of ^{131}I-absorbed Au NPs was assessed in vivo by H&E staining of major organs, including the heart, liver, spleen, lungs, and kidneys. No apparent lesions, inflammation, or tissue damage in the major organ sections were observed after the various treatments, similar to the saline control (Figure S3). Moreover, there was no significant difference in the biochemical parameters of the ICR mice treated with ^{131}I@PEI-Au NPs, PEI-Au NPs and saline (Table S1). These results exhibited the good biosafety profile of the generated ^{131}I-absorbed Au NPs, which did not exert apparent toxicity in vivo.

Despite the efficient radiolabeling, high in vitro stability, and good in vivo therapeutic effects of ^{131}I-absorbed Au NPs, the limitations of this work should also be acknowledged. First, given the diversity of Au NPs and iodine isotopes (such as ^{123}I, ^{124}I, and ^{125}I), additional researches need to be conducted to support the universality of chemisorption between them. Second, the in vivo instability of ^{131}I-absorbed Au NPs probably related to the selected Au NPs in this study, and can be solved by developing more robust and elaborate Au NPs. Third, although the lack of good stability and targeting ability in vivo makes the ^{131}I-absorbed Au NPs unsuitable for intravenous injection, it still could be developed as novel approaches for cancer treatment, such as through intratumoral injection, peritumoral injection or embolization. Furthermore, the characteristic of specific adsorption and desorption might endow radioiodine-absorbed Au NPs with significant potential for broader applications, such as the selective recognition and separation of radioiodine from radioactive waste liquids.

Conclusion

In summary, chemisorption between Au NPs and ^{131}I ion is instant, specific, and quantitative. ^{131}I-absorbed Au NPs with high RCPs can be prepared by simply mixing the two components. Au NPs with different surface modifications, including glucose, PEG, BSA, and PEI, could still absorb ^{131}I efficiently. The prepared ^{131}I-absorbed Au NPs exhibited long-term stability under different conditions and satisfactory inhibitory effects for tumor cells in vitro. Despite some degree of instability in vivo, ^{131}I-absorbed Au NPs showed remarkable therapeutic efficacy and a good biosafety profile in a tumor-bearing mouse model after intratumoral injection. Considering the variety of iodine isotopes with different emission properties, Au NPs could be used as a powerful nanoplatform for imaging and radionuclide therapy; the characteristic of specific adsorption and desorption might also endow radioiodine-absorbed Au NPs with significant potential for broader applications.

Funding

This research was funded by the Jiangsu Shuangchuang Talents Plan (SC0001), Ningxia Key Research and Development Program (2020BFG03005), Jiangsu Provincial Health Commission General Project (H2023055), Jiangsu Provincial Medical Key Discipline Cultivation Unit (JSDW202251) and “Lvyang Jinfeng” talents attracting plan (LYJF00040).

Disclosure

The authors declare no conflicts of interest in this work.

References

1. Hope TA, Pavel M, Bergsland EK. Neuroendocrine tumors and peptide receptor radionuclide therapy: when is the right time? *J Clin Oncol*. 2022;40 (24):2818–2829. doi:10.1200/jco.22.00176

2. Gill MR, Falzone N, Du Y, Vallis KA. Targeted radionuclide therapy in combined-modality regimens. *Lancet Oncol*. 2017;18(7):e414–e423. doi:10.1016/S1470-2045(17)30379-0
3. Yang C, Gao Y, Fan Y, et al. Dual-mode endogenous and exogenous sensitization of tumor radiotherapy through antifouling dendrimer-entrapped gold nanoparticles. *Theranostics*. 2021;11(4):1721–1731. doi:10.7150/thno.54930
4. Sgouros G, Bodei L, McDevitt MR, Nedrow JR. Radiopharmaceutical therapy in cancer: clinical advances and challenges. *Nat Rev Drug Discov*. 2020;19(9):589–608. doi:10.1038/s41573-020-0073-9
5. Sun J, Huangfu Z, Yang J, et al. Imaging-guided targeted radionuclide tumor therapy: from concept to clinical translation. *Adv Drug Deliv Rev*. 2022;190:114538. doi:10.1016/j.addr.2022.114538
6. Su W, Chen C, Wang T, et al. Radionuclide-labeled gold nanoparticles for nuclei-targeting internal radio-immunity therapy. *Mater Horiz*. 2020;7(4):1115–1125. doi:10.1039/C9MH01725A
7. Pomykala KL, Hadaschik BA, Sartor O, et al. Next generation radiotheranostics promoting precision medicine. *Ann Oncol*. 2023;34(6):507–519. doi:10.1016/j.annonc.2023.03.001
8. Song G, Cheng L, Chao Y, Yang K, Liu Z. Emerging nanotechnology and advanced materials for cancer radiation therapy. *Adv Mater*. 2017;29(32):1700996. doi:10.1002/adma.201700996
9. Pan Y, Tang W, Fan W, Zhang J, Chen X. Development of nanotechnology-mediated precision radiotherapy for anti-metastasis and radioprotection. *Chem Soc Rev*. 2022;51(23):9759–9830. doi:10.1039/D1CS01145F
10. Llop J, Lammers T. Nanoparticles for cancer diagnosis, radionuclide therapy and theranostics. *ACS Nano*. 2021;15(11):16974–16981. doi:10.1021/acsnano.1c09139
11. Pellico J, Gawne PJ, de Rosales RT. Radiolabelling of nanomaterials for medical imaging and therapy. *Chem Soc Rev*. 2021;50(5):3355–3423. doi:10.1039/D0CS00384K
12. Yook S, Cai Z, Lu Y, et al. Intratumorally injected ^{177} lu-labeled gold nanoparticles: gold nanoseed brachytherapy with application for neoadjuvant treatment of locally advanced breast cancer. *J Nucl Med*. 2016;57(6):936–942. doi:10.2967/jnumed.115.168906
13. An J, He X, Ma H, et al. Radionuclide labeled nanocarrier for imaging guided combined radionuclide, sonodynamic, and photothermal therapy of pancreatic tumours. *J Colloid Interface Sci*. 2023;642:789–799. doi:10.1016/j.jcis.2023.03.111
14. Medici S, Peana M, Coradduzza D, Zoroddu MA. Gold nanoparticles and cancer: detection, diagnosis and therapy. *Semin Cancer Biol*. 2021;76:27–37. doi:10.1016/j.semcancer.2021.06.017
15. Li R, Li D, Jia G, et al. Diagnostic performance of theranostic radionuclides used in transarterial radioembolization for liver cancer. *Front Oncol*. 2021;10:551622. doi:10.3389/fonc.2020.551622
16. Goas ML, Paquet M, Paquirissamy A, et al. Improving ^{131}I Radioiodine Therapy By Hybrid Polymer-Grafted Gold Nanoparticles. *Int J Nanomed*. 2019;14:7933–7946. doi:10.2147/IJN.S211496
17. Zhao L, Li Y, Zhu J, et al. Chlorotoxin peptide-functionalized polyethylenimine-entrapped gold nanoparticles for glioma SPECT/CT imaging and radionuclide therapy. *J Nanobiotechnology*. 2019;17(1):30. doi:10.1186/s12951-019-0462-6
18. Zhang Y, Zhang Y, Yin L, et al. Synthesis and bioevaluation of iodine-131 directly labeled cyclic RGD-PEGylated gold nanorods for tumor-targeted imaging. *Contrast Media Mol Imaging*. 2017;2017:6081724. doi:10.1155/2017/6081724
19. Zhu J, Zhao L, Zhao P, et al. Charge-conversional polyethylenimine-entrapped gold nanoparticles with ^{131} I-labeling for enhanced dual mode SPECT/CT imaging and radiotherapy of tumors. *Biomater Sci*. 2020;8(14):3956–3965. doi:10.1039/D0BM00649A
20. Cheng D, Gong J, Wang P, et al. ^{131}I-Labeled gold nanoframeworks for radiotherapy-combined second near-infrared photothermal therapy of cancer. *J Mater Chem B*. 2021;9(45):9316–9323. doi:10.1039/D1TB02115J
21. Huang S, Zhang L, Xu M, et al. Co-delivery of ^{131}I and prima-1 by self-assembled CD44-targeted nanoparticles for anaplastic thyroid carcinoma theranostics. *Adv Healthc Mater*. 2021;10(3):2001029. doi:10.1002/adhm.202001029
22. Na Sun LZ, Zhu J, Yujie L, et al. ^{131}I-labeled polyethylenimine-entrapped gold nanoparticles for targeted tumor SPECT/CT imaging and radionuclide therapy. *Int J Nanomed*. 2019;14:4367–4381. doi:10.2147/IJN.S203259
23. Kelly G, Milligan JJ, Mastria EM, et al. Intratumoral delivery of brachytherapy and immunotherapy by a thermally triggered polypeptide depot. *J Control Release*. 2022;343:267–276. doi:10.1016/j.jconrel.2022.01.024
24. Walsh AA. Chemisorption of iodine-125 to gold nanoparticles allows for real-time quantitation and potential use in nanomedicine. *J Nanopart Res*. 2017;19(4):152. doi:10.1007/s11051-017-3840-8
25. Shao X, Agarwal A, Rajian JR, Kotov NA, Wang X. Synthesis and bioevaluation of ^{125}I-labeled gold nanorods. *Nanotechnology*. 2011;22(13):135102. doi:10.1088/0957-4484/22/13/135102
26. Hortelao AC, Simó C, Guix M, et al. Swarming behavior and in vivo monitoring of enzymatic nanomotors within the bladder. *Sci Rob*. 2021;6(52):eabd2823. doi:10.1126/scirobotics.abd2823
27. Wang R, Liu H, Antal B, Wolterbeek HT, Denkova AG. Ultrasmall gold nanoparticles radiolabeled with iodine-125 as potential new radiopharmaceutical. *Acs Appl Bio Mater*. 2024;7(2):1240–1249. doi:10.1021/acsabm.3c01158
28. Ghosh S, Banerjee D, Guleria A, Chakravarty R. Production, purification and formulation of nanoradiopharmaceutical with ^{211}At: an emerging candidate for targeted alpha therapy. *Nucl Med Biol*. 2024;138:108947. doi:10.1016/j.nucmedbio.2024.108947
29. Tanudji J, Kasai H, Okada M, et al. ^{211} At on gold nanoparticles for targeted radionuclide therapy application. *Phys Chem Chem Phys*. 2024;26(17):12915–12927. doi:10.1039/D3CP05326A
30. Huang X, Kaneda-Nakashima K, Kadonaga Y, et al. Astatine-211-labeled gold nanoparticles for targeted alpha-particle therapy via intravenous injection. *Pharmaceutics*. 2022;14(12):2705. doi:10.3390/pharmaceutics14122705
31. Mignani S, Shi X, Ceña V, et al. Engineered non-invasive functionalized dendrimer/dendron-entrapped/complexed gold nanoparticles as a novel class of theranostic (radio)pharmaceuticals in cancer therapy. *J Control Release*. 2021;332:346–366. doi:10.1016/j.jconrel.2021.03.003
32. Yang Y, Zheng X, Chen L, et al. Multifunctional gold nanoparticles in cancer diagnosis and treatment. *Int J Nanomed*. 2022;17:2041–2067. doi:10.2147/IJN.S355142
33. Poletto G, Evangelista L, Venturini F, et al. Nanoparticles and radioisotopes: a long story in a nutshell. *Pharmaceutics*. 2022;14(10):2024. doi:10.3390/pharmaceutics14102024
34. Pulagam KR, Henriksen-Lacey M, Uribe KB, et al. In vivo evaluation of multifunctional gold nanorods for boron neutron capture and photothermal therapies. *ACS Appl Mater Interfaces*. 2021;13(42):49589–49601. doi:10.1021/acsami.0c17575

35. Li C, Zhao L, Jia L, et al. ^{68}Ga-labeled dendrimer-entrapped gold nanoparticles for PET/CT dual-modality imaging and immunotherapy of tumors. *J Mater Chem B*. 2022;10(19):3648–3656. doi:10.1039/D2TB00378C
36. Zhou B, Wang R, Chen F, et al. ^{99m}Tc-labeled rgd–polyethylenimine conjugates with entrapped gold nanoparticles in the cavities for dual-mode SPECT/CT imaging of hepatic carcinoma. *ACS Appl Mater Interfaces*. 2018;10(7):6146–6154. doi:10.1021/acsami.7b17107
37. Pulagam KR, Gona KB, Gómez-Vallejo V, et al. Gold nanoparticles as boron carriers for boron neutron capture therapy: synthesis, radiolabelling and in vivo evaluation. *Molecules*. 2019;24(19):3609. doi:10.3390/molecules24193609
38. Clanton R, Gonzalez A, Shankar S, Akabani G. Rapid synthesis of ^{125}I integrated gold nanoparticles for use in combined neoplasm imaging and targeted radionuclide therapy. *Appl Radiat Isot*. 2018;131:49–57. doi:10.1016/j.apradiso.2017.10.030
39. Chen F, Wang M, Du Z, Pu X, Zhu B. ^{131}I labeled pH-responsive gold nanoparticles for bimodal tumor diagnosis. *Mater Lett*. 2023;330:133202. doi:10.1016/j.matlet.2022.133202
40. Black KCL, Wang Y, Luehmann HP, et al. Radioactive ^{198}Au-doped nanostructures with different shapes for in vivo analyses of their biodistribution, tumor uptake, and intratumoral distribution. *ACS Nano*. 2014;8(5):4385–4394. doi:10.1021/nn406258m
41. Zhao Y, Pang B, Luehmann H, et al. Gold nanoparticles doped with ^{199}Au atoms and their use for targeted cancer imaging by SPECT. *Adv Healthc Mater*. 2016;5(8):928–935. doi:10.1002/adhm.201500992
42. Chakravarty R, Chakraborty S, Guleria A, et al. Clinical scale synthesis of intrinsically radiolabeled and cyclic RGD peptide functionalized ^{198}Au nanoparticles for targeted cancer therapy. *Nucl Med Biol*. 2019;72:1–10. doi:10.1016/j.nucmedbio.2019.05.005
43. Chakravarty R, Sen N, Ghosh S, et al. Flow synthesis of intrinsically radiolabeled and renal-clearable ultrasmall [^{198}Au]Au nanoparticles in a PTFE microchannel. *Chem Eng J Adv*. 2023;14:100456. doi:10.1016/j.ceja.2023.100456
44. Chakravarty R, Chakraborty S, Guleria A, et al. Facile one-pot synthesis of intrinsically radiolabeled and cyclic RGD conjugated ^{199}Au nanoparticles for potential use in nanoscale brachytherapy. *Ind Eng Chem Res*. 2018;57(43):14337–14346. doi:10.1021/acs.iecr.8b02526
45. Shukla R, Chanda N, Zambre A, et al. Laminin receptor specific therapeutic gold nanoparticles (^{198}AuNP-EGCg) show efficacy in treating prostate cancer. *Proc Natl Acad Sci U S A*. 2012;109(31):12426–12431. doi:10.1073/pnas.1121174109
46. Chanda N, Kan P, Watkinson LD, et al. Radioactive gold nanoparticles in cancer therapy: therapeutic efficacy studies of GA-^{198}AuNP nanoconstruct in prostate tumor–bearing mice. *Nanomed-Nanotechnol*. 2010;6(2):201–209. doi:10.1016/j.nano.2009.11.001